Available online at www.sciencedirect.com
SCIENCE DIRECT®
Proceedings of the Combustion Institute 30 (2005) 2851–2858
Proceedings of the Combustion Institute
www.elsevier.com/locate/proci

Combustion oscillations in a scramjet engine combustor with transverse fuel injection

Jeong-Yeol Choi[a,*], Fuhua Ma[b], Vigor Yang[b]

[a] *Pusan National University, Busan 609-735, Republic of Korea*
[b] *The Pennsylvania State University, University Park, PA 16802, United States*

Abstract

A comprehensive numerical analysis has been carried out for both non-reacting and reacting flows in a scramjet engine combustor with and without a cavity. Transverse injection of hydrogen is considered over a broad range of injection pressure. The corresponding equivalence ratio of the overall fuel/air mixture ranges from 0.167 to 0.50. The work features detailed resolution of the flow and flame dynamics in the combustor, which was not typically available in most of the previous studies. In particular, the oscillatory flow characteristics are captured at a scale sufficient to identify the underlying physical mechanisms. Much of the flow unsteadiness is related not only to the cavity, but also to the intrinsic unsteadiness in the flowfield. The interactions between the unsteady flow and flame evolution may cause a large excursion of flow oscillation. The roles of the cavity, injection pressure, and heat release in determining the flow dynamics are examined systematically.

Keywords: Supersonic combustion; Combustion instability; Air-breathing propulsion; Scramjet engine; Computational fluid dynamics

1. Introduction

The success of future high-speed air transportation will be strongly dependent on the development of hypersonic air-breathing propulsion engines. Although there exist many fundamental issues, combustor represents one of the core technologies that dictate the development of hypersonic propulsion systems. At a hypersonic flight speed, the flow entering the combustor should be maintained supersonic to avoid the excessive heating and dissociation of air. The residence time of the air in a hypersonic engine is on the order of 1 ms for typical flight conditions. The fuel must be injected, mixed with air, and burned completely within such a short time span.

A number of studies have been carried out worldwide, and various concepts have been suggested for scramjet combustor configurations to overcome the limitations given by the short flow residence time. Among the various injection schemes, transverse fuel injection into a channel type of combustor appears to be the simplest and has been used in several engine programs, such as the Hyshot scramjet engine, an international program lead by the University of Queensland [1]. For the enhancement of fuel/air mixing and flame-holding, a cavity is often employed. For example, the CIAM of Russia introduced cavities into its engines [2] and US Air Force also employed cavities in the supersonic combustion experiments [3].

* Corresponding author. Fax: +1 82 51 513 3760.
E-mail address: aerochoi@pusan.ac.kr (J.-Y. Choi).

1540-7489/$ - see front matter
doi:10.1016/j.proci.2004.08.250

From the aspect of fluid dynamics, transverse injection of fluid into a supersonic cross-flow and flow unsteadiness associated with a cavity are of significant interest due to their broad applications in many engineering devices. Extensive efforts have been applied to study these phenomena, and much of the results have great relevance to scramjet combustors. A comprehensive study directly applied to combustor dynamics, however, is rarely found. The obstacles lie in the difficulties in conducting high-fidelity experiments and numerical simulations to characterize the flow transients at time and length scales sufficient to resolve the underlying mechanisms. The present study attempts to achieve improved understanding of the unsteady flow and flame dynamics in a realistic scramjet combustor configuration employing a transverse fuel injection and a flame holding cavity. Little is known about this issue from the previous studies.

2. Theoretical formulation and numerical treatment

2.1. Governing equations

The flowfield is assumed to be two-dimensional for computational efficiency, and can be described with the conservation equations for a multi-component chemically reactive system. The coupled form of the species conservation, fluid dynamics, and turbulent transport equations can be summarized in a conservative vector form as follows:

$$\frac{\partial \mathbf{Q}}{\partial t}+\frac{\partial \mathbf{F}}{\partial x}+\frac{\partial \mathbf{G}}{\partial y}=\frac{\partial \mathbf{F_v}}{\partial x}+\frac{\partial \mathbf{G_v}}{\partial y}+\mathbf{W}, \tag{1}$$

where the conservative variable vector, $\mathbf{Q}$, convective flux vectors, $\mathbf{F}$ and $\mathbf{G}$, diffusion flux vectors, $\mathbf{F_v}$ and $\mathbf{G_v}$, and reaction source term $\mathbf{W}$ are defined in Eqs. (2a) and (2b). Details of the governing equations and thermophysical properties are described in [4]:

$$\mathbf{Q}=\begin{bmatrix}\rho_i\\ \rho u\\ \rho v\\ e\\ \rho k\\ \rho\omega\end{bmatrix},\quad \mathbf{F}=\begin{bmatrix}\rho_i u\\ \rho u^2+p\\ \rho uv\\ (e+p)u\\ \rho ku\\ \rho\omega u\end{bmatrix},\quad \mathbf{G}=\begin{bmatrix}\rho_i v\\ \rho uv\\ \rho v^2+p\\ (e+p)v\\ \rho kv\\ \rho\omega v\end{bmatrix}, \tag{2a}$$

$$\mathbf{F_v}=\begin{bmatrix}-\rho_i u_i^d\\ \tau_{xx}\\ \tau_{xy}\\ \beta_x\\ \mu_k\partial k/\partial x\\ \mu_\omega\partial\omega/\partial x\end{bmatrix},\quad \mathbf{G_v}=\begin{bmatrix}-\rho_i v_i^d\\ \tau_{xy}\\ \tau_{yy}\\ \beta_y\\ \mu_k\partial k/\partial y\\ \mu_\omega\partial\omega/\partial y\end{bmatrix},\quad \mathbf{W}=\begin{bmatrix}w_i\\ 0\\ 0\\ 0\\ S_1\\ S_2\end{bmatrix}, \tag{2b}$$

where i denotes species i, ranging from *1* to N.

2.2. Chemistry model and turbulence closure

The present analysis employs the GRI-Mech 3.0 chemical kinetics mechanism for hydrogen–air combustion [5]. The mechanism consists of eight reactive species (H, H_2, O, O_2, H_2O, OH, H_2O_2, and HO_2) and 25 reaction steps. Nitrogen is assumed as an inert gas because its oxidation process has only a minor effect on the flame evolution in a combustor. Turbulence closure is achieved by means of Mentor's shear stress transport (SST) model derived from the k–ω two-equation formulation [6]. This model is the blending of the standard k–ε model that is suitable for a shear layer problem and the Wilcox k–ω model that is suitable for wall turbulence effect [7]. Baridna et al. [8] reported that the SST model offers good prediction for mixing layers and jet flows, and is less sensitive to initial values in numerical simulations.

Another important issue is the closure problems for the interaction of turbulence and chemistry in supersonic conditions. Recently, there were many attempts to address this issue using LES methods, PDF approaches, and other combustion models extended from subsonic combustion conditions. Although much useful advances were achieved, the improvement was insignificant in comparison with the results obtained from laminar chemistry and experimental data, as discussed by Möbus et al. [9]. A careful review of existing results, such as Norris and Edwards [10], suggests that the solution accuracy seems to be more dependent on grid resolution than the modeling of turbulence–chemistry interaction. In view of the lack of reliable models for turbulence–chemistry interactions, especially for supersonic flows, the effect of turbulence on chemical reaction rate is ignored in the present work.

2.3. Numerical methods

The governing equations were treated numerically using a finite volume approach. The convective fluxes were formulated using Roe's FDS method derived for multi-species reactive flows along with the MUSCL approach utilizing a differentiable limiter function. The spatial discretization strategy satisfies the TVD conditions and features a high-resolution shock capturing capability. The discretized equations were temporally integrated using a second-order accurate, fully implicit method. A Newton sub-iteration method was also used to preserve the time accuracy and solution stability. Detailed descriptions of the governing equations and numerical formulation are documented in a previous work [11].

2.4. Code verification

The overall approach has been validated against a number of steady and unsteady flow

problems including shock-induced combustion oscillation. Good agreement has been obtained with experimental data [12,13]. In addition, numerical study was carried out to validate the present turbulence modeling and to justify the grid resolution for simulating transverse gas injection across the supersonic flow over a flat plate. The analysis simulates the experiment described in [14] with a static pressure ratio of 10.29, for which several numerical studies have been previously carried out [15,16]. In this case, choked nitrogen flow is vertically injected through a 1-mm-wide slot located 33 cm behind the leading edge into a supersonic airflow with a Mach number of 3.75. The present study used the same computational domain as that of Chenault and Beran [16]. Computations were carried out for various combinations of grid systems having 71–351 points near the injection port in the streamwise direction and 41–251 points clustered near the wall in the transverse direction. Furthermore, a parametric study was performed on the effects of numerical and turbulence modeling parameters. The numerical parameters were optimized to maintain numerical stability and solution convergence. The turbulence parameters of the SST model [6] have negligible effects on the solutions for the grid systems employed herein.

Figure 1 compares the wall-pressure distributions between the numerical and experimental results. A coarse grid results in a longer separation distance ahead of the injection port and cannot predict the pressure picks near the injection port, although the solution seems to better match the experimental result. The 281×201 and 351×251 grids have nearly identical results within 5% relative error range over the entire wall. In comparison with previous results, the present turbulence model predicts the same separation distance and peak pressure as the k–ϵ model while maintaining smooth pressure increase in the front separation region. Also, pressure variation behind the injector is more closely predicted by the SST model. The 281×201 grid was then applied to the scramjet combustor simulation. The minimum vertical spacing is $y^+ \leqslant 5$, and 21 grid points are employed in the injector port.

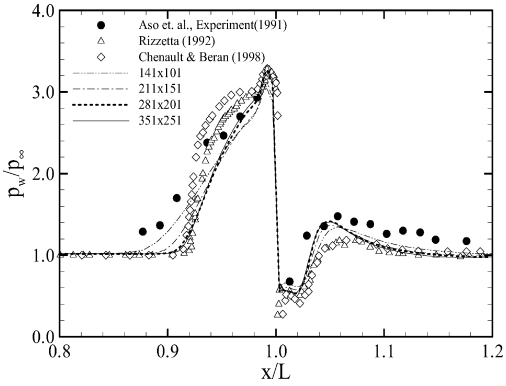

Fig. 1. Wall pressure distribution of the two-dimensional transverse injection across the supersonic flow over a flat plate.

3. Scramjet combustor

3.1. Combustor geometry

The supersonic combustor considered in this study is shown in Fig. 2, consisting of a transverse fuel injector and a cavity. The model measures a height of 20 cm and a length of 131 cm. The configuration bears a close resemblance to the Hyshot test model, except for the inclusion of a cavity. A swallowing slot is employed to remove the boundary layer from the inlet, and the combustor starts with a sharp nose [1]. A cavity of 20 cm in length and 5 cm in depth, with an aspect ratio of $L/D = 4.0$, is placed at 20 cm downstream of the injector.

3.2. Operating conditions

The incoming air flow to the combustor is set to a Mach number of 3 at 600 K and 0.1 MPa. This inlet condition roughly corresponds to a flight Mach number of 5–6 at an altitude of 20 km, although the exact condition depends on the inlet configuration. Gaseous hydrogen is injected vertically through a chocked slot of 0.1 cm in width to the combustor. The fuel temperature is set to 151 K. The injector exit pressures are 0.5, 1.0, and 1.5 MPa, and the overall equivalence ratios are 0.167, 0.33, and 0.5.

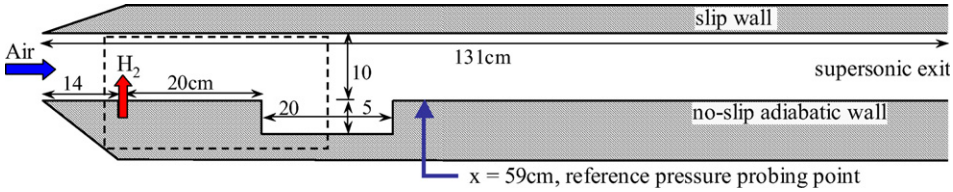

Fig. 2. Scramjet combustor configuration.

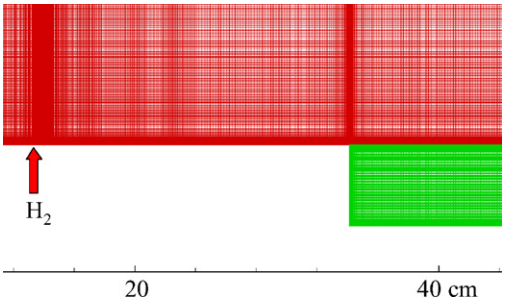

Fig. 3. Magnified plot of computational grid around the injector and the upstream part of the cavity.

3.3. Combustor conditions

A total of 936×160 grids are used for the main-combustor flow passage, and 159×161 grids for the cavity. The grids are clustered around the injector and near the solid wall. Fifty four grid points are included in the injector slot, and the minimum grid size near the wall is 70 μm. All the solid surfaces are assumed to be no-slip and adiabatic, except for the upper boundary, which is assumed to be a slip wall due to flow symmetric condition. Extrapolation is used to extract flow properties for the exit boundary. The time step is set to 6 ns according to the minimum grid size for a CFL number of 2.0. Four sub-iterations are used at each time step. Figure 3 is a magnified plot of the computational grid around the injector and the fore part of the cavity marked by the dashed line in Fig. 2.

4. Results and discussion

Numerical simulations were carried out for 12 cases, including both non-reacting and reacting flows, with and without the cavity, for three different injection pressures of 0.5, 1.0, and 1.5 MPa. The following sections will discuss the results for each case. All the calculations were performed for 6 ms from the initial condition, which is longer than the typical test time of ground based experiments. The instantaneous flowfields shown in the following were taken at $t = 5$ ms.

4.1. Non-reacting flows without cavity

Figure 4 shows the instantaneous temperature fields for the non-reacting flows without a cavity. For the injection pressure ratio of 5.0, the flowfield around the injector seems to be quite stable, but a flow disturbance is observed at the location around 40 cm where the first reflected shock wave interacts with the shear layer between the fuel and air flows. The disturbance propagates upstream through the shear layer, but does not reach the injector. The injector flow thus remains stable, and the fuel flow is located very close to the lower surface. The mechanism of the shear layer instability, which is triggered by the impinging oblique shock wave, seems to be the one studied by Papamoschou and Roshko [17].

For the injection pressure ratio of 10.0, disturbance was generated during the early stage of the computation in a manner similar to the case of the injection pressure ratio of 5.0. It, however, propagates upstream and triggers the injector flow to become unstable. As a result, a large portion of the flow area becomes subsonic and the injector flow oscillates strongly. The unstable motion leads to a higher fuel penetration and substantially enhanced fuel/air mixing. This injector flow instability mechanism has previously been observed by Papamoschou and Hubbard [18]. Ben-Yakar et al. [19] found essentially the same phenomenon in their supersonic combustion experiment. As the injection pressure ratio further increases to 15.0, the injector flow instability is getting stronger and flow oscillations take place in the entire combustor. The fuel penetrates to the middle of the combustor and the mixing with the air is greatly enhanced.

Figure 5 shows the temporal variation of the pressure at the location of $x = 59$ cm from the leading edge of the lower surface. This location

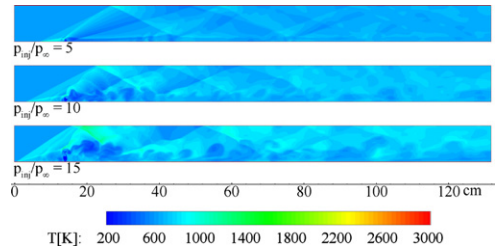

Fig. 4. Instantaneous temperature fields at 5 ms for non-reacting flows without a cavity.

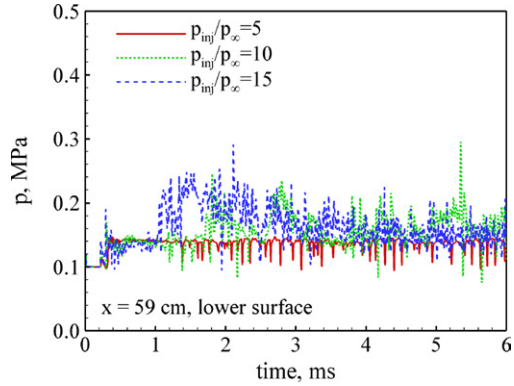

Fig. 5. Time history of pressure for non-reacting flows without a cavity.

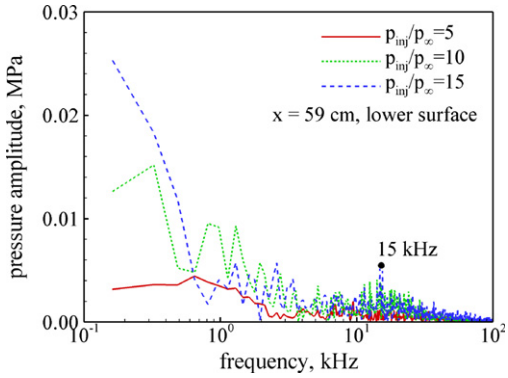

Fig. 6. Frequency spectra of pressure oscillations for non-reacting flows without a cavity.

is 5 cm downstream of the cavity, and is selected because of its reflection of all the instability characteristics discussed above. The curve for the injection pressure ratio of 5.0 shows oscillations generated by the interactions between the shock wave and boundary layer. Similar results are obtained for the high injection pressures. The flowfield, however, becomes considerably unstable at 1.8 ms for the pressure ratio of 10.0 and at 1.0 ms for the pressure ratio of 15.0. Steady oscillations are then reached, after a transitional period of 1–2 ms. Figure 6 shows the frequency spectra of the pressure oscillations. A dominant frequency exists around 15 kHz for the injection pressure ratios of 10.0 and 15.0.

4.2. Non-reacting flows with cavity

Figure 7 shows the instantaneous temperature fields for non-reacting flows with a cavity in the chamber. In general, the cavity generates disturbances which propagate upstream and in turn trigger the injector flow instability, even for the case with a low injection pressure ratio of 5.0. Thus, the flowfields exhibit considerable oscillations for all the injection pressure ratios considered here. The fuel penetration and subsequent mixing with air are greatly enhanced by the cavity-driven flow oscillations.

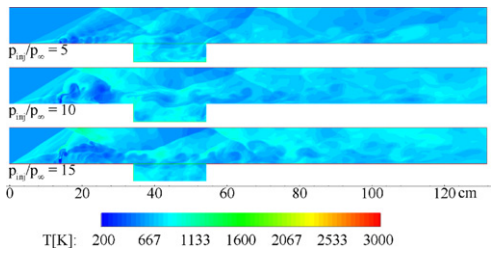

Fig. 7. Instantaneous temperature fields at 5 ms for the case of non-reacting flows with a cavity.

Figure 8 shows the pressure–time histories at the location of $x = 59$ cm. For all the three injection pressure ratios, the injector flow instability starts to occur at 1 ms, which is around the half of the value for the cases without a cavity. Also, the pressure fluctuation is much stronger with its mean value maintained slightly higher than the cases without a cavity. Figure 9 shows the frequency spectra of pressure oscillations. Unlike the case without a cavity, the dominant frequency decreases from 15 kHz to around 1.5–2.5 and 4–6 kHz. The specific value depends on the injection pressure ratio. The intrinsic frequencies of the cavity oscillation predicted by a Rossiter's semi-empirical formula and discussed by Ben-Yakar and Hanson [20] are 1.9 kHz for the first mode and 4.5 kHz for the second mode based on the flow conditions considered in this study. Thus, the present computational simulations give quite satisfactory results, considering the complex flow structures involving shock waves and fuel injection.

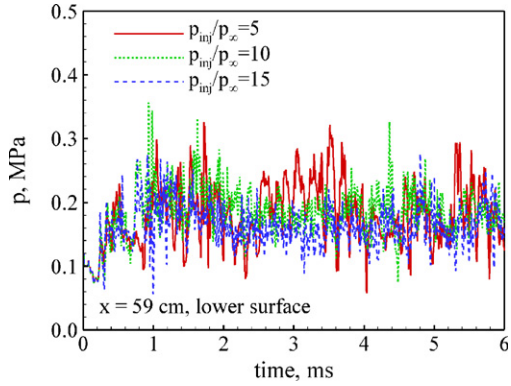

Fig. 8. Temporal variation of pressure for non-reacting flows with a cavity.

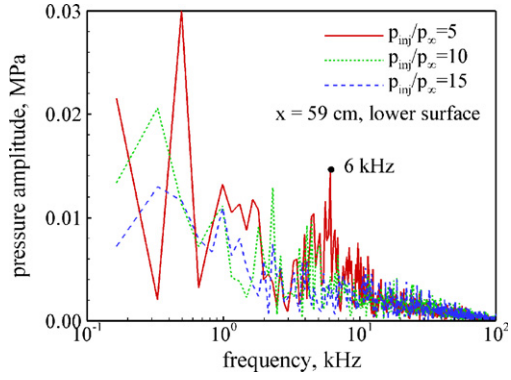

Fig. 9. Frequency spectra of pressure oscillations for non-reacting flows with a cavity.

4.3. Reacting flows without cavity

Figure 10 shows the instantaneous temperature fields for reacting flows without a cavity. For the injection pressure ratio of 5.0, combustion occurs in the frontal separation region, but is not fully established along the shear layer. This separation region contains a pool of radicals and acts as a preheating zone. The flame is not anchored there, but in the region containing shock-wave/shear-layer interactions where the instability occurs. Downstream of this location, heat release from chemical reactions takes place, accompanied with large vortices convecting downstream. The overall phenomena seem quite similar to a typical turbulent diffusion flame generating large vorticities. It is thought from this result that chemical reactions do not intensify the disturbance to an extent sufficient for triggering the instability of the injector flow.

The temperature fields exhibit different characteristics for the injection pressure ratios of 10.0 and 15.0. As a consequence of the large heat release, the pressure behind the injector builds up and leads to a Mach reflection across the combustor. A large subsonic region is thus formed downstream of the injector, and the injector flow no longer shows a structure comprising of a leading oblique shock wave, a frontal separation region, etc. Instead, the fuel is injected though a narrow width of a subsonic port, but can penetrate much deeper. The frontal separated flow region, which acts as a radical pool and a pre-heater, still exists for the injection pressure ratio of 10.0, but disappears for a higher pressure ratio of 15.0 due to the fully subsonic environment near the injector. The frontal separated flow region and the oblique shock wave extend to the leading edge of the combustor and are stabilized there by the fixed inlet boundary condition.

Figure 11 shows the temporal evolution of the pressure for the reacting flows without a cavity. For the injection pressure ratio of 5.0, the final pressure is slightly higher than that of the non-reacting case and the pressure builds up very slowly. In contrast, the results for the pressure ratios of 10.0 and 15.0 indicate that the injector flow instability is triggered around 1 ms and the pressure levels off at approximately 0.5 MPa around 3 ms for the pressure ratio of 10.0, and at 0.6 MPa around 1.5 ms for the ratio of 15.0. Figure 12 shows the frequency spectra of pressure oscillations. Unlike the non-reacting cases, no dominant frequency is observed, and the spectra are widely distributed.

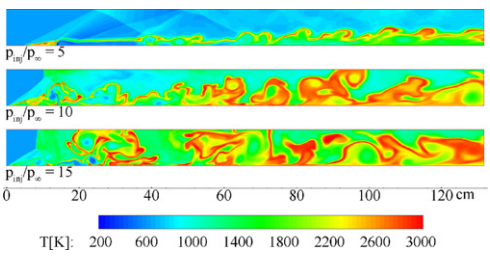

Fig. 10. Instantaneous temperature fields at 5 ms for reacting flows without a cavity.

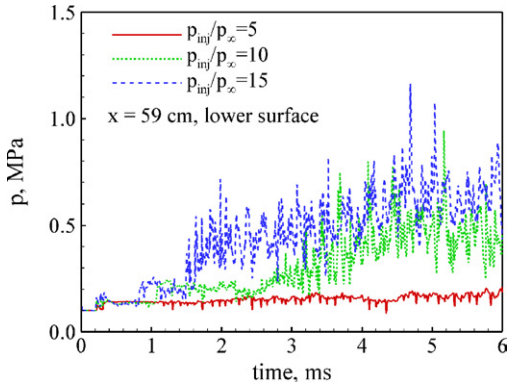

Fig. 11. Pressure–time histories for reacting flows without a cavity.

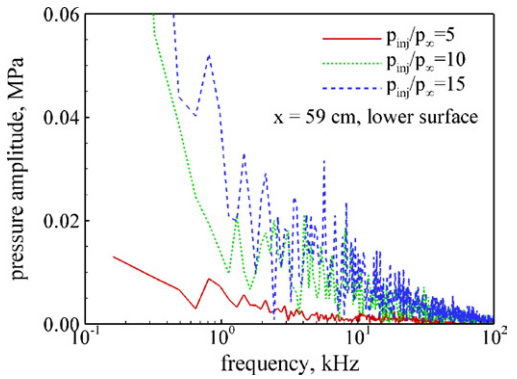

Fig. 12. Frequency spectra of pressure oscillations for reacting flows without a cavity.

4.4. Reacting flows with cavity

Figure 13 shows the instantaneous temperature fields for the reacting flows with a cavity. For the injection pressure ratio of 5.0, combustion is fully established over the cavity, which acts as a flame holder or a radical pool. The chamber pressure reaches around 0.3 MPa, much greater than the case without a cavity. For the injection pressure ratios of 10.0 and 15.0, the pressure builds up rapidly and eventually leads to thermal chocking in the chamber. The Mach reflection continuously develops and is finally disgorged out of the inlet. The pressure–time history shown in Fig. 14 indi-

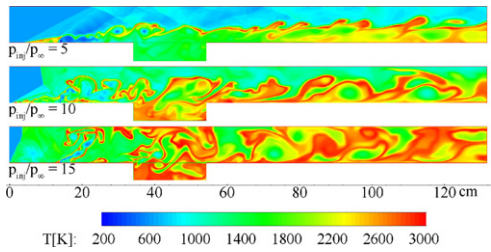

Fig. 13. Instantaneous temperature fields at 5 ms for reacting flows with a cavity.

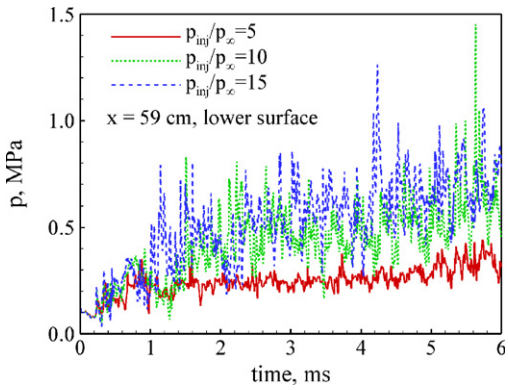

Fig. 14. Pressure–time histories for reacting flows with a cavity.

cated that the combustion is established much earlier than the cases without a cavity for all the injection pressure ratios. This may be attributed to the mixing and combustion enhancement by the cavity, a phenomenon that can be understood by comparing the pressure variations in Figs. 8 and 11. The frequency spectra in Fig. 15 exhibit a broad distribution without any major dominant harmonics, similar to the cases without a cavity.

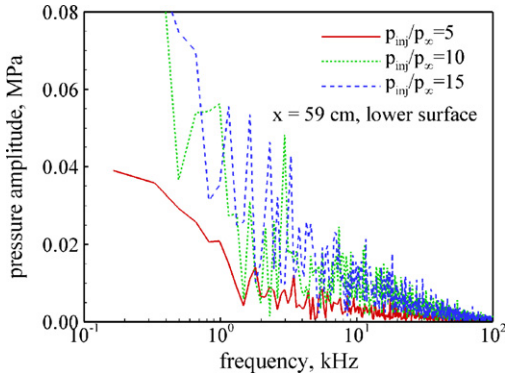

Fig. 15. Frequency spectra of pressure oscillations for reacting flows with a cavity.

5. Conclusion

The non-reacting and reacting flow dynamics in a scramjet combustor was carefully studied by means of a comprehensive numerical analysis. The results show a wide variety of phenomena resulting from the interactions between the injector flows, shock waves, boundary layers, and cavity flows. Major findings are summarized as follows:

1. Strong unsteady flow characteristics were identified for a scramjet combustor. The work appears to be the first of its kind in the numerical study of combustion oscillations in a supersonic combustor.
2. Large flow disturbances can be generated by shear layer instability that may be triggered by the interactions with shock waves.
3. For all the cases studied herein, flow oscillations caused by the cavity override those induced by the interactions between shock waves and boundary layers.
4. Transverse injected jet can be triggered to become unstable with disturbances arising from a shear layer or a cavity. The disturbed jet can penetrate deeper into the cross-flow and improve the mixing with air. A more detailed study is necessary to characterize the stability of a transverse injected jet.
5. The roles of the cavity as a source of disturbance for the transverse jet oscillation, fuel/air mixing enhancement, and flame-holding improvement were clarified.
6. Unstable flow characteristics for the reacting cases bear a close resemblance to those of non-reacting flows except for a rapid chamber pressure build-up to a higher level.
7. When the combustion takes place throughout the entire chamber, an unstable Mach reflection is formed above the injector due to the flow unsteadiness and results in a strong pressure fluctuation on the upper wall.
8. As an extreme case of high pressure build-up, thermal choking occurs in the combustor, which may result in the combustor unstart due to the forward-running strong shock wave.
9. The present study can be extended to a more realistic combustor configuration, but further investigations are required to achieve better understanding of detailed fluid and flame dynamics in a scramjet combustor.

References

[1] Centre for Hypersonics—HyShot Scramjet Test Programme. Available from http://www.mech.uq.edu.au/hyper/hyshot/.

[2] C. McClinton, A. Roudakov, V. Semenov, V. Kopehenov, *AIAA Paper* 96-4571, 1996.
[3] T. Mathur, M. Gruber, K. Jackson, J. Donbar, W. Donaldson, T. Jackson, F. Billig, *J. Prop. Power* 17 (6) (2001) 1305–1312.
[4] J.Y. Choi, I.S. Jeung, Y. Yoon, *AIAA J.* 36 (6) (1998) 1029–1038.
[5] G.P. Smith, D.M. Golden, M. Frenklach, N.W. Moriarty, B. Eiteneer, M. Goldenberg, C.T. Bowman, R.K. Hanson, S. Song, W.C. Gardiner, V.V. Lissianski, Z. Qin, GRI-Mech. Available from: <http://www.me.berkeley.edu/gri_mech/>.
[6] F.R. Menter, *AIAA J.* 32 (8) (1994) 1598–1605.
[7] D.C. Wilcox, Turbulence Modeling for CFD, DCW Industries, La Cañada, CA, 1993.
[8] J.E. Bardina, P.G. Huang, T.J. Coakly, *AIAA Paper* 1997-2121, 1997.
[9] M. Möbus, P. Gerlinger, D. Brüggermann, *Combust. Flame* 132 (1) (2003) 3–24.
[10] J.W. Norris, J.R. Edwards, *AIAA Paper* 1997-0370, 1997.
[11] J.Y. Choi, I.S. Jeung, Y. Yoon, *AIAA J.* 38 (7) (2000) 1179–1187.
[12] J.Y. Choi, I.S. Jeung, Y. Yoon, *AIAA J.* 37 (5) (1999) 537–543.
[13] J.Y. Choi, I.S. Jeung, Y. Yoon, *Proc. Combust. Inst.* 27 (1998) 2181–2188.
[14] S. Aso, K. Okuyama, S. Kawai, Y. Ando, *AIAA Paper* 1991-0016, 1991.
[15] D. Rizzetta, *AIAA Paper* 1992-0827, 1992.
[16] C.F. Chenault, P.S. Beran, *AIAA J.* 36 (8) (1998) 1401–1412.
[17] D. Papamoschou, A. Roshko, *J. Fluid Mech.* 197 (1988) 453–477.
[18] D. Papamoschou, D.G. Hubbard, *Exper. Fluids* 14 (1993) 468–471.
[19] A. Ben-Yakar, M.R. Kamel, C.I. Morris, R.K. Hanson, *AIAA Paper* 1997-3019, 1997.
[20] A. Ben-Yakar, R.K. Hanson, *J. Prop. Power* 17 (4) (2001) 869–877.

Comment

In-Seuck Jeung, Seoul National University, Korea. Would you comment on the application of boundary layer control on the isolator area to mitigate the large separation region due to the pre-combustion shock-boundary layer interaction? Would you suggest this boundary layer control might reduce the strength of the flow unsteadiness?

Reply. The flow unsteadiness observed in the present study can be classified into two categories: intrinsic flow instabilities and thermo-fluidic instability. The intrinsic flow instabilities include supersonic cavity flow oscillations and Richtmyer–Meshkov instability in shock-wave/shear-layer interactions. The thermo-fluidic instability is caused by combustor choking for large-heat-addition cases. The results show that the intrinsic flow instabilities have high-frequency low-amplitude oscillations but the thermo-fluidic instability causes only large-scale motions. A large separation region ahead of the injector was present in every case considered, but was irrelevant to intrinsic instabilities. We are not sure whether the boundary layer control can reduce the strength of the flow unsteadiness induced by intrinsic instabilities, although we agree that it may mitigate the large separation region. On the other hand, the thermal choking is caused by the overall thermodynamic balance in the combustor, rather than a local flow dynamics. Therefore we could not expect that the boundary layer control can mitigate the flow unsteadiness induced by thermal choking. Though not shown in the paper, a precursor shock wave that progresses forward due to combustor choking will blow off the large separation region eventually.